A window on exoplanet dynamical histories: Rossiter-McLaughlin observations of WASP-13b and WASP-32b

Journal Item

Version: Version of Record

Link(s) to article on publisher's website:
http://dx.doi.org/doi:10.1093/mnras/stu520

Mon. Not. R. Astron. Soc. **000**, 000–000 (0000) Printed 18 March 2014 (MN LATEX style file v2.2)

A Window on Exoplanet Dynamical Histories: Rossiter-McLaughlin observations of WASP-13b and WASP-32b

R. D. Brothwell[1⋆], C. A. Watson[1], G. Hébrard[2,3], A. H. M. J. Triaud[4,5], H. M. Cegla[1], A. Santerne[6], E. Hébrard[7], D. R. Anderson[8], D. Pollacco[9], E. K. Simpson[1], F. Bouchy[2,3], D. J. A. Brown[9], Y. Gómez Maqueo Chew[9], A. Collier Cameron[10], D. J. Armstrong[9], S. C. C. Barros[11], J. Bento[9,12], J. Bochinski[13], V. Burwitz[14], R. Busuttil[13], L. Delrez[15], A. P. Doyle[8], F. Faedi[9], A. Fumel[15], M. Gillon[15], C. A. Haswell[13], C. Hellier[8], E. Jehin[15], U. Kolb[13], M. Lendl[4], C. Liebig[10], P. F. L. Maxted[8], J. McCormac[16,9], G. R. M. Miller[10], A. J. Norton[13], F. Pepe[4], D. Queloz[17], J. Rodríguez[18], D. Ségransan[4], I. Skillen[16], B. Smalley[8], K. G. Stassun[19,20], S. Udry[4], R. G. West[9], P. J. Wheatley[9]

[1] *Astrophysics Research Centre, School of Mathematics & Physics, Queen's University Belfast, BT7 1NN, UK*
[2] *Institut d'Astrophysique de Paris, UMR7095 CNRS, Université Pierre & Marie Curie, France*
[3] *Observatoire de Haute-Provence, CNRS/OAMP, 04870 St Michel l'Observatoire, France*
[4] *Observatoire astronomique de l'Université de Genève, 51 ch. des Maillettes, 1290 Sauverny, Switzerland*
[5] *Department of Physics, and Kavli Institute for Astrophysics and Space Research, Massachusetts Institute of Technology, Cambridge, MA 02139, USA*
[6] *Centro de Astrofisica, Universidade do Porto, Rua das Estrellas, 4150-762, Porto, Portugal*
[7] *IRAP-UMR 5277, CNRS and Univ. de Toulouse, 14 Av. E. Belin, F-31400, Toulouse, France*
[8] *Astrophysics Group, Keele University, Staffordshire, ST5 5BG, UK*
[9] *Department of Physics, University of Warwick, Coventry, CV4 7AL*
[10] *School of Physics and Astronomy, University of St Andrews, North Haugh, St Andrews, Fife KY16 9SS, UK*
[11] *Aix Marseille Université, CNRS, LAM (Laboratoire d'Astrophysique de Marseille) UMR 7326, 13388, Marseille, France*
[12] *Department of Physics and Astronomy, Macquarie University, NSW 2109, Australia*
[13] *Department of Physical Sciences, The Open University, Milton Keynes, MK7 6AA, UK*
[14] *Max Planck Institut für Extraterrestrische Physik, Giessenbachstrasse 1, 85748 Garching, Germany*
[15] *Université de Liège, Allée du 6 août 17, Sart Tilman, Liège 1, Belgium*
[16] *Isaac Newton Group of Telescopes, Apartado de Correos 321, E-38700 Santa Cruz de Palma, Spain*
[17] *Department of Physics, University of Cambridge, J J Thomson Av, Cambridge, CB3 0HE, UK*
[18] *Observatori Astronòmic de Mallorca, Camí de l'Observatori s/n 07144 Costitx, Mallorca, Spain*
[19] *Physics and Astronomy Department, Vanderbilt University, Nashville, Tennessee 37235, USA*
[20] *Department of Physics, Fisk University, Nashville, Tennessee 37208, USA*

Accepted 2014 March 12. Received 2014 March 12; in original form 2013 November 25

ABSTRACT

We present Rossiter-McLaughlin observations of WASP-13b and WASP-32b and determine the sky-projected angle between the normal of the planetary orbit and the stellar rotation axis (λ). WASP-13b and WASP-32b both have prograde orbits and are consistent with alignment with measured sky-projected angles of $\lambda = 8^{\circ}{}^{+13}_{-12}$ and $\lambda = -2^{\circ}{}^{+17}_{-19}$, respectively.

Both WASP-13 and WASP-32 have $T_{\rm eff} < 6250$K and therefore these systems support the general trend that aligned planetary systems are preferentially found orbiting cool host stars. A Lomb-Scargle periodogram analysis was carried out on archival SuperWASP data for both systems. A statistically significant stellar rotation period detection (above 99.9% confidence) was identified for the WASP-32 system with $P_{\rm rot} = 11.6 \pm 1.0$ days. This rotation period is in agreement with the predicted stellar rotation period calculated from the stellar radius, $R_{\star}$, and $v \sin i$ if a stellar inclination of $i_{\star} = 90^{\circ}$ is assumed. With the determined rotation period, the true 3D angle between the stellar rotation axis and the planetary orbit, ψ, was found to be $\psi = 11^{\circ} \pm 14$. We conclude with a discussion on the alignment of systems around cool host stars with $T_{\rm eff} < 6150$K by calculating the tidal dissipation timescale. We find that systems with short tidal dissipation timescales are preferentially aligned and systems with long tidal dissipation timescales have a broad range of obliquities.

Key words: stars: planetary systems – stars: individual: WASP-13 –WASP-32– techniques: radial velocities – techniques: photometric

1 INTRODUCTION

The study of gas giants orbiting close to their host stars allows an insight into the formation and evolution of exoplanets. For example, combined planetary transit photometry and radial velocity (RV) measurements enables the planetary density to be found, providing constraints on the planetary composition. Whilst this provides clues to the formation processes at work, the Rossiter-McLaughlin (RM) effect is thought to be a complementary probe of exoplanet dynamical histories. The RM effect is measured using in-transit spectroscopic observations, revealing a deviation from the Keplerian orbital motion as the star orbits the barycentre of the star-planet system. The effect is caused by the planet occulting the rotating stellar surface. This introduces an asymmetry in the stellar absorption profile, resulting in an apparent shift of the spectral lines. The RM waveform allows the sky projected spin-orbit alignment angle (λ) between the rotation axis of the host star and the normal to the planetary orbital plane to be determined.

The alignment angle is thought to provide a window on the dynamical evolution of exoplanets. Hot-Jupiters are thought to form beyond the snow-line where icy cores become massive enough to accrete a gaseous envelope before subsequently migrating either via planet-disk, planet-planet or planet-star interactions. Planet-disk interactions are thought to be dynamically gentle (Goldreich & Tremaine 1980; Lin, Bodenheimer & Richardson 1996) and do not peturb the original inclination of the planet. Other migration mechanisms such as planet-planet and planet-star interactions via the Kozai-Lidov mechanism are more dynamically violent (Kozai 1962; Lidov 1962). The presence of a third body in the system excites periodic oscillations in the eccentricity and inclination of the orbit, where tidal dissipation and circularisation shrinks the semi-major axis. The oscillating inclination resulting from Kozai-Lidov interactions produces a continuum of inclinations with stable orbits. Thus, it is expected that hot-Jupiters will exhibit misaligned orbits if such migration processes are operating.

However, it should be noted that measuring a spin-orbit alignment angle of $\lambda = 0^{\circ}$ does not necessarily indicate an aligned planetary system. When the impact parameter is low, the RM waveform is independent of λ and instead controls the amplitude, leading to a strong degeneracy between $v \sin i$ and λ (Gaudi & Winn 2007). For example, in a system with an impact parameter of $b = 0$ and/or where the stellar rotation axis is inclined in the direction of the observer, any orientation of the planetary orbit leads to a symmetric RM waveform. By calculating the inclination of the stellar rotation axis, these degeneracies can be broken and the true '3D' system geometry ascertained.

Currently, 76[1] planets have a measured λ where 45% of planets show substantial misalignments. This population of misaligned planets appears to be synonymous with hotter host stars ($T_{\rm eff} \geqslant 6250$K) whilst aligned planets are preferentially observed orbiting cool host stars. One proposed reason for the alignment-misalignment transition is a change in the internal structure of main-sequence host stars around 6250K, where the outer convective envelope is responsible for tidal interactions. Another correlation in current RM data is the degree of alignment with system age (Triaud 2011). All systems with $M_{\star} \geqslant 1.2$ $M_{\odot}$ were considered and systems with ages greater than 2.5 Gyrs are preferentially aligned, whereas those below this age are preferentially misaligned. This reflects the development of the convective envelope with system age and lends further support to alignment arising from tidal interactions. Albrecht et al. (2012) showed that other correlations of alignment with the orbital period, ratio of planet mass to stellar mass and possibly orbital distance with λ provide further evidence that realignment is driven by tidal interactions.

In order to interpret the results of RM observations as a tracer of dynamical evolution alone, it must be assumed that the original protoplanetary disk and the star are well-aligned. While this seems valid based on angular momentum conservation, theoretical models have begun to challenge this assumption, showing that star-disk misalignment is possible in the pre-mainsequence phase (Bate, Lodato & Pringle 2010; Lai, Foucart & Lin 2011). Thus, measuring λ may not trace planet migration mechanisms but perhaps traces star formation processes or a combination of both. Watson et al. (2011) studied the inclination of resolved debris disks and the inclination of their host stars for 9 systems, showing that all are consistent with alignment. The authors note that all systems have $T_{\rm eff} < 6250$K and other candidates with $T_{\rm eff} > 6250$K would be important in exploring the full alignment-misalignment theoretical picture proposed by Winn et al. (2010). Further systems, with a range of spectral types, were investigated by Greaves et al. (2014) where the stellar inclination was found to be aligned with the spatially resolved debris disk for all systems. Recently Kennedy et al. (2013) tested the alignment of the full star-disk-planet system for HD 82943, the first time the full alignment of a system has been investigated. The complete system (the inclination of the stellar rotation axis, the normal to the disk plane and the normal to the planetary orbit) was found to be aligned at a level similar to the Solar System.

Another approach to distinguish between primordial star-disk misalignments and misalignment driven by migration is to consider the growing number of multiplanet systems. Albrecht et al. (2013) recently analysed the multiple-transiting systems KOI-94 (Hirano et al. 2012) and Kepler-25, finding $\lambda = -11 \pm 11^{\circ}$ and $\lambda = 7 \pm 8^{\circ}$, results consistent with alignment. Whilst this was thought to hint that multi-planet systems migrate via planet-disk interactions and hot-Jupiters migrate by a different pathway, evidence for misaligned multi-planet systems has been found (Huber et al. 2013; Walkowicz & Basri 2013). It is clear that a full picture of hot-Jupiter formation and migration is far from complete, requiring the continual buidling of statistics, preferably beyond the $T_{\rm eff}$ dependence, to explore unstudied regions of parameter space.

In this paper we report Rossiter-McLaughlin (RM) observations of WASP-13 and WASP-32. WASP-13 and WASP-32 are both slow rotators (Skillen et al. 2009; Maxted et al. 2010) and cool stars with effective temperatures $\sim$6000K. Section 2 outlines the observations and analysis procedure. In Section 3 the derived parameters are presented and discussed. Next a search for the stellar rotation period for both systems was investigated. For WASP-32, where a period was found, we then computed the true 3D alignment angle. Finally, we conclude with a discussion of our results in Section 4.

[1] Holt-Rossiter-McLaughlin Encyclopaedia:
http://www.physics.mcmaster.ca/$\sim$rheller/

Table 1. Adopted system parameters and uncertainties used to model the RM effect, and other photometric parameters used in this work. The reference is indicated at the end of the column for each object.

Parameter (units)	Symbol	WASP-13	WASP-32
Orbital Period (days)	P	4.3530135 ± 0.0000027	2.718659 ± 0.000008
Transit epoch	T_0	$2455305.62823 \pm 0.00025$ ($\mathrm{BJD_{UTC}}$)	2455151.0546 ± 0.0005 (HJD)
Transit duration (hours)	T_d	4.003 ± 0.024	2.424 ± 0.048
Orbital inclination (°)	i	85.43 ± 0.29	85.3 ± 0.5
Planet/Star radius ratio	R_p/R_*	0.0919 ± 0.0126	0.11 ± 0.01
Scaled semi-major axis	a/R_*	7.54 ± 0.27	7.63 ± 0.35
Eccentricity	e	0 (adopted)	0.0180 ± 0.0065
Reference		Gómez Maqueo Chew et al. (2013)	Maxted et al. (2010)

2 DATA ANALYSIS

2.1 Observations and data reduction

All in-transit radial velocity (RV) data for WASP-13 and WASP-32 were obtained using the SOPHIE spectrograph mounted on the 1.93m telescope at the Observatoire Haute Provence (OHP). SOPHIE is an environmentally stabilised echelle spectrograph (wavelength range 382-693nm) designed for high-precision RV measurements. Two 3 arcsecond optical fibres were used, with one centred on the target and the other used to simultaneously monitor the sky background in case of lunar light contamination. The spectra were then reduced using the SOPHIE data reduction pipeline (Perruchot et al. 2008). Radial velocities were extracted using a weighted cross-correlation of each spectrum with a G2 spectral-type mask. A Gaussian was then fitted to the resulting cross-correlation functions to obtain the radial velocity shift. Uncertainities were computed using the empirical relation of Bouchy et al. (2009) and Cameron et al. (2007). The observation and data reduction details particular to each system are presented in Section 3.

2.2 Determination of the system parameters

The RM effect and orbit were fitted simultaneously using all the available spectroscopic data, including previously published orbital data. A Keplerian model was used for the orbit, and the analytical approach described in Ohta, Taruya & Suto 2005 (hereafter OTS) was used to model the RM effect. An independent systemic velocity was fitted to each orbital dataset in order to account for any instrumental offsets. Similarly the transit datasets were fitted with separate systemic velocities to incorporate instrumental and long-term stellar activity variations.

To fit the RM effect the OTS equations were modified to make them dependent on R_p/R_* and a/R_* rather than R_p, R_* and a, to reflect the parameters derived from photometry, and reduce the number of free parameters. The model comprises 11 parameters: the orbital period, P; mid-transit time, T_0; planetary to stellar radius ratio, R_p/R_*; scaled semi-major axis, a/R_*; orbital inclination, i; orbital eccentricity, e; longitude of periastron, ω; radial velocity semi-amplitude of the host star, K; sky projected angle between the stellar rotation axis and orbital angular momentum vector, λ; projected stellar rotational velocity, $v \sin i$ and the stellar linear limb-darkening coefficient, u.

In summary, the OTS model assumes that the star and transiting planet are disks where the planet is an opaque occulting disk. The radial velocity of a small element on the stellar disk is given by multiplying the x-position of the element (Figure 3 of OTS) by $v \sin i$. This quantity is then weighted by the intensity of the stellar disc at that location and then all the elements are integrated over the entire stellar surface. The OTS equations (see sections 5.1 and 5.2 of OTS) result from assuming a linear limb darkening law for the stellar intensity. A linear limb darkening law is assumed as the quadratic model is known to deviate by only a few m $\mathrm{s}^{-1}$from the linear limb darkening model. Also, it has been shown that by setting u as a free parameter, λ and $v \sin i$ are not significantly affected (Simpson et al. 2011).

A series of parameters included in the model have been derived previously from transit observations (P, R_p/R_*, a/R_* and i_p). These constraints can be included in the fit in the form of a χ^2 penalty function:

$$\chi^2 = \sum_i \left[\frac{v_{i,\mathrm{obs}} - v_{i,\mathrm{calc}}}{\sigma_i}\right]^2 + \left(\frac{X - X_{\mathrm{obs}} + [\sigma_{X_{\mathrm{obs}}} \times G(0,1)]}{\sigma_{X_{\mathrm{obs}}}}\right)^2 \quad (1)$$

where $v_{i,\mathrm{obs}}$ and $v_{i,\mathrm{calc}}$ are the ith observed and calculated radial velocities from the model, respectively, and σ_i is the corresponding observational error. X is one of the fitted parameters and X_{obs} is the fitted parameter determined from other observations where $\sigma_{X_{\mathrm{obs}}}$ is the associated error. The multiplicative factor $G(0,1)$ is a Gaussian randomly generated number with a mean of 0 and a standard deviation of 1. This includes in the fit the error determined from prior observations. Equation 1 was extended to include all constraints on all parameters where prior parameter information is known. The procedure is described on a case by case basis for each object in the following sections.

To find the best-fitting solution a chi-squared minimisation was carried out using the IDL function MPFIT, utilizing the Levenburg-Marquart algorithm. The 1σ best-fit parameter uncertainties were calculated using a Monte-Carlo method. 10^5 synthetic data sets were created by adding a 1σ Gaussian random variable multiplied by the error on the radial velocity to the radial velocity data points. The free parameters were re-optimised for each simulated data-set to obtain the distribution of the best-fit parameter values. The distributions were not as-

sumed to be Gaussian and the 1σ limits were found where the distribution enclosed $\pm 34.1\%$ of the values away from the median. As a consistency check, the data were also analysed using the RML fitting procedure used by, for example, Hébrard et al. (2011a) and Moutou et al. (2011).

3 ANALYSIS

3.1 WASP-13

WASP-13b is a sub-Jupiter mass exoplanet with $M_{\rm p} = 0.500 \pm 0.037 M_{\rm J}$ and $R_p = 1.407 \pm 0.052 R_{\rm J}$ with an orbital period of 4.4 days (Gómez Maqueo Chew et al. 2013). Its host star is a G1V type with $T_{\rm eff} = 5989 \pm 48$K, $M_\star = 1.187 \pm 0.065 {\rm M}_\odot$, $\log g = 4.16$ and solar metallicity. The host star has a projected rotational velocity of $v \sin i = 5.74 \pm 0.38$ km s^{-1}(Gómez Maqueo Chew et al. 2013).

A transit of WASP-13b was observed with the SOPHIE spectrograph at the 1.93-m telescope at the Observatoire de Haute-Provence (OHP) on the night of 2012 March 6. We acquired a total of 54 spectra, 32 spectra in-transit and 22 spectra out-of-transit with a total of 228 minutes of out-of-transit data (primarily post-transit). SOPHIE was used in high efficiency mode (HE) with a resolution of $R = 40,000$ and fast read-out mode, maintaining a constant signal to noise throughout the observing run ($S/N = 30$). Typical exposure times were 600s and the seeing remained $\sim$2 arcseconds during the observing night. The measured radial velocities are listed in Table 3. Moon illumination was 97% and at a distance of $\sim$30 degrees from WASP-13 on the night of observation. We note that the lunar RV was 0.002 km s^{-1}which, when compared to the systemic velocity of WASP-13 of $\gamma_{\rm orbit} = 9.8345 \pm 0.0031$ km s^{-1}, means most of the lunar contribution lies outside the stellar absorption-line profile. Nevertheless, we have applied the standard lunar contamination correction available through the SOPHIE data reduction pipeline. To fit the orbit, we used 11 SOPHIE observations acquired during the discovery of the planet (Skillen et al. 2009). The fitted orbit can be found in the left hand panel of Figure 1 with the fitted systemic velocity $\gamma_{\rm orbit} = 9.8345 \pm 0.0031$ km s^{-1}removed from the RV datapoints.

To fit the RM effect the OTS model was used as described in Section 2.2. The fitted RM waveform can be found in the right hand panel of Figure 1 with the systemic velocity $\gamma_{\rm transit} = 9.7854 \pm 0.0037$ km s^{-1}removed from the RV datapoints. In the model the linear limb darkening coefficient was chosen from the tables of Claret (2004) (ATLAS models) for the g' filter. A linear interpolation using John Southworth's JKTLD code with stellar parameters of $T_{\rm eff} = 5989$K, $[M/H] = 0.06$, $\log g = 4.16$, $v_{\rm mic} = 1.27$ km s^{-1}was used and a linear limb-darkening coefficient of $u = 0.75$ was adopted. The eccentricity was fixed at $e = 0$ and a constraint on $v \sin i = 5.74 \pm 0.38$ km s^{-1}was added to the χ^2 penalty function (Gómez Maqueo Chew et al. 2013).

A χ^2 statistic was adopted of the form of Equation 1 where the priors included in the penalty function are listed in Table 1. The fitted parameters and uncertainties are given in Table 5. The best-fitting model is shown in Figure 1 where $\lambda = 8^{\circ}{}^{+13}_{-12}$. It is clear from the shape of Figure 1 that the planet has a prograde orbit. In addition, the RV waveform shows a symmetric shape indicating star-planet alignment. A fit was also attempted with no prior on $v \sin i$ with no effect on the fitted parameters. This is explained by the large impact parameter ($b = 0.6$) where the degeneracy between λ and $v \sin i$ only becomes important in the low impact parameter regime. In this regime the form of the RM signal is not strongly dependent on λ, however the amplitude is controlled by both λ and $v \sin i$. It has been shown that applying a penalty function in this regime has no overall impact on the fitted parameters (Simpson et al. 2011) and this is indeed what we found in the case of WASP-13.

3.2 WASP-32

WASP-32 is a massive exoplanet with $M_p = 3.60 \pm 0.07 {\rm M}_{\rm J}$ and $R_p = 1.19 \pm 0.06 R_{\rm J}$ in a $P = 2.7$ day orbit. The host star has $T_{\rm eff} = 6100 \pm 100$K, $M_\star = 1.10 \pm 0.03 {\rm M}_\odot$, $\log g = 4.4$ and is lithium depleted (Maxted et al. 2010). The projected rotational velocity of the host star is $v \sin i = 4.8 \pm 0.8$ km s^{-1}(Maxted et al. 2010).

We acquired 22 spectra during the transit of WASP-32, covering the complete transit. 4 spectra were acquired prior to transit and 8 spectra were acquired post transit with a total of 168 mins of observations acquired outside transit. The data were obtained using SOPHIE on the night of 2011 August 29th, with clear conditions and a typical seeing of 2.5 arcseconds. SOPHIE was operated in high-efficiency mode and there was no moonlight pollution on the night of observation. The derived radial velocities can be found in Table 4. To fit the orbit 14 CORALIE out-of-transit RVs were used from the WASP-32 discovery paper (Maxted et al. 2010). The fitted orbit can be found in the left hand panel of Figure 2 with the systemic velocity offset $\gamma_{\rm orbit} = 18.2796^{+0.0061}_{-0.0062}$ km s^{-1}removed from the RV data points.

To fit the RM effect the OTS model was used as described in Section 2.2. The fitted RM waveform can be found in the right hand panel of Figure 2 with the systemic velocity $\gamma_{\rm transit} = 18.1698 \pm 0.0095$ km s^{-1}removed from the RV data points. We note the difference in the orbital and transit systemic velocities is ~ 100 m s^{-1}for WASP-32 and $\sim$50 m s^{-1}for WASP-13, comparable to values obtained for other objects in the literature. In particular, Simpson et al. (2010) measured a difference in the orbital and transit velocities for WASP-1b of $\sim$200 m s^{-1}using the same RM model and observational approach. Also we examined the likelihood that the measured systemic velocity offsets could be driven by long-term stellar activity by phase-folding the WASP-13 and WASP-32 light-curves with the transits removed. A clear sinusoidal photometric modulation was detected in the light-curve for WASP-32 at the $\sim$2% level, although modulations were not detected for WASP-13. The increased activity level of WASP-32 also explains why a period peak was detected in the periodogram (discussed in Section 3.3). Using the relation presented in Saar & Donahue (1997) the RV shift due to inhomogeneous spot coverage can be estimated. A $\sim$100 m s^{-1}RV shift for WASP-32 is expected with $\sim$2% inhomogeneous spot coverage, comparable to the difference in our reported systemic velocity for WASP-32 compared to the systemic velocity of the orbital data. Therefore, the difference in systemic velocities may be explained by spot coverage. It is important to note that the RM effect duration for WASP-32 is $\sim$2.4 hours, during which the host star rotates by $\sim$8 degrees. Thus, it is unlikely new spot features would rotate into view during transit, and thus systemic velocity offsets over the course of the RM observation are insignificant. In the model the linear

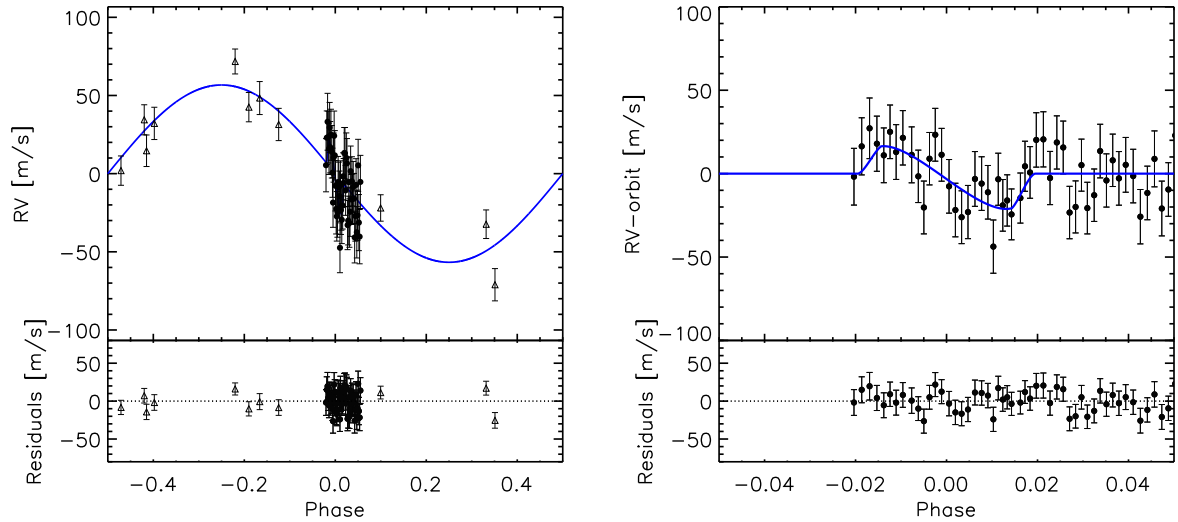

Figure 1. *Left Panel:* WASP-13 phase-folded orbit minus the systemic velocity overplotted with the best-fitting model (solid line). Out-of-transit radial velocities of Skillen et al. (2009) are displayed as open triangles and the measured radial velocities using SOPHIE at the OHP on the night March 6 2012 are displayed as filled circles. *Right Panel:* Spectroscopic transit minus the orbital velocity, overplotted with the best-fitting RM model with the residuals shown below.

limb darkening coefficient was chosen as before with stellar parameters of $T_{\rm eff} = 6100$K, $[M/H] = -0.13$, $\log g = 4.39$, $v_{\rm mic} = 2$ km s^{-1}, resulting in a linear limb darkening coefficient of $u = 0.71$. WASP-32 is a reasonably eccentric system with $e = 0.018 \pm 0.0065$ and this parameter was fixed in the RM fit.

A χ^2 statistic was adopted of the form of Equation 1, where the priors included in the penalty function are taken from Maxted et al. (2010) and are listed in Table 1. The best fitting model is shown in Figure 2 where $\lambda = -2^{\circ}{}^{+17}_{-19}$ and the fitted parameters are listed in Table 6. It is clear from Figure 2 that WASP-32 has a symmetric RM waveform, moving from redshift to blueshift, consistent with an aligned prograde orbit. The fitted λ is consistent with that found recently by Brown et al. (2012) where $\lambda = 10.5^{\circ}{}^{+6.4}_{-5.9}$.

The fitted $v \sin i = 7.6^{+4.2}_{-3.1}$ km s^{-1}is consistent with that found from sprectroscopic fitting, $v \sin i = 4.8 \pm 0.8$ km s^{-1}(Maxted et al. 2010) and the measured $v \sin i = 3.9^{+0.4}_{-0.5}$ km s^{-1}derived from Doppler Tomography (Brown et al. 2012). However, our determined $v \sin i$ is noticeably larger than the others that have been found. Thus, a fit with a prior on $v \sin i$ set to that found by Brown et al. (2012) was attempted. It was found that λ is insensitive to fixing $v \sin i$ in the fit, with little change in $\chi^2_{\rm red}$. Thus, the fit with a prior on $v \sin i$ was taken as our adopted solution with a fitted $\lambda = -2^{\circ}{}^{+17}_{-19}$ and $v \sin i = 3.9 \pm 0.5$ km s^{-1}. Also we attempted a fit using the Brown et al. (2012) HARPS RVs alone and found that the error bars on λ were increased relative to the Brown et al. (2012) results. We attribute this to the use of simultaneous photometry in the Brown et al. (2012) analysis but note our fit is the first independent analysis on the alignment of WASP-32b.

3.3 3D Alignment Angle

Modelling the Rossiter-McLaughlin effect leads to a determination of the sky-projected alignment angle, λ. As a consequence of only measuring the sky-projected alignment angle, in some cases a measured λ that indicates an aligned planet may actually be a misaligned system. For example, measuring a $\lambda = 0^{\circ}$ does not necessarily indicate an aligned planetary system if the inclination of the stellar rotation axis is unknown. If the stellar rotation axis is inclined relative to the line of sight or if the impact parameter, b, is close to 0 then the planet may be misaligned but the symmetry of the RM waveform would indicate an aligned system. A true three dimensional reconstruction of the system geometry can be gleaned if the inclination of the host star can be found simultaneously with the sky-projected angle, removing any possible ambiguities that remain from RM observations alone.

By determining the stellar rotation period ($P_{\rm rot}$) combined with the projected rotational velocity ($v \sin i$) and stellar radius ($R_\star$), the stellar inclination ($i_\star$) can be found via:

$$\sin i_\star = P_{\rm rot} \times \left(\frac{v \sin i_\star}{2\pi R_\star} \right) \quad (2)$$

The projected stellar rotational velocity, $v \sin i$, and stellar radius estimates can be obtained via spectral analysis. There are a number of ways to determine the stellar rotation period, to determine $i_\star$, either by monitoring Ca H and K emission or photometric monitoring of starspots (e.g. Simpson et al. 2010, Watson et al. 2010). In our analysis we adopt the latter, where the modification of disk integrated light indicates the passage of starspots across the stellar surface. By sourcing the detrended WASP lightcurves for WASP-13 and WASP-32, an extensive Lomb-Scargle (Lomb 1976; Scargle 1982) periodogram analysis was carried out to search for significant stellar rotation periods. The significance of the periods was estimated using the false alarm probability (FAP- Horne & Baliunas 1986). A detection was defined when the peak in the periodogram surpassed the 0.1% FAP power level. This means the detected period has a 99.9% confidence level that it does not arise by chance. Before carrying out the periodogram analysis on all sourced light curves, the updated transit ephemeris was used to remove the planetary transits. This prevented unwanted harmonics entering the periodograms and ensured intrinsic stellar periodicities were analysed. As a useful comparison, assuming the rotation

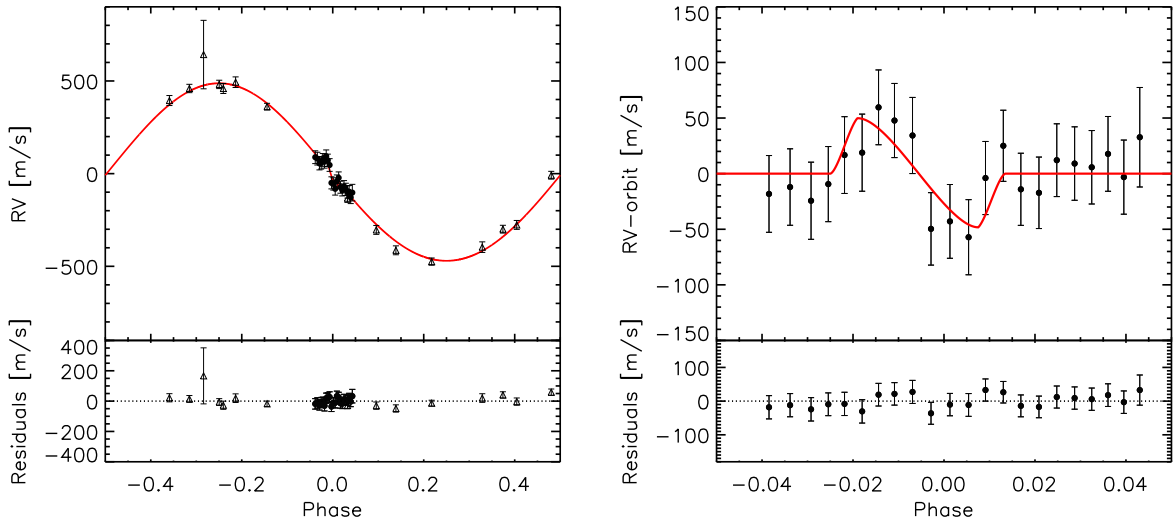

Figure 2. *Left Panel:* WASP-32 phase-folded orbit minus the systemic velocity overplotted with the best-fitting model (solid line). Out-of-transit radial velocities of Maxted et al. (2010) from CORALIE are displayed as open triangles and the measured radial velocities using SOPHIE are displayed as filled circles. *Right Panel:* Spectroscopic transit minus the orbital velocity, overplotted with the best-fitting RM model with the residuals shown below.

axis is perpendicular to the line of sight ($i_\star = 90°$), $P_{\rm rot}$ can be computed for all three systems using the $v \sin i$ quoted for all three systems in Section 3. In the case of WASP-32 a number of $v \sin i$ measurements have been determined but we use $v \sin i = 3.9^{+0.4}_{-0.5}$ km s^{-1}from Doppler Tomography (Brown et al. 2012) to compute the stellar inclination for WASP-32. For WASP-13 and WASP-32, true alignment would lead to expected values of the stellar rotation period of $P_{\rm rot} = 17.1$ and 11.7 days, respectively. No statistically significant rotation period was detected for WASP-13, however a statistically significant period was detected in the WASP-32 data above the 99.9% confidence level. The detected period is $P_{\rm rot} = 11.6 \pm 1.0$ days and the periodogram is shown in Figure 3. With $P_{\rm rot}$ known, $i_\star$ can be determined from equation 5, where an $i_\star = 81° \pm 9$ was found. This, combined with the planetary inclination (i_p) determined from the planetary transit and λ, allows the true 3D alignment angle, ψ, to be found via:

$$\cos\psi = \cos i_\star \cos i_p + \sin i_\star \sin i_p \cos\lambda \quad (3)$$

The measured 3D alignment angle, using $\lambda = 10.5^{\circ+6.4}_{-5.9}$ from Brown et al. (2012) gives $\psi = 11° \pm 14$ and using the value of $\lambda = -2^{\circ+17}_{-19}$, derived in this work, $\psi = 2° \pm 16$. Both results indicate that the planet is aligned when considered as a 3D system.

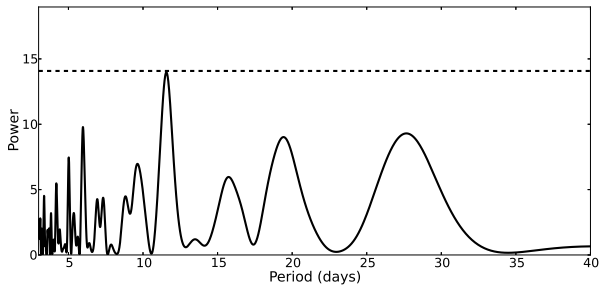

Figure 3. Lomb-Scargle periodogram analysis for the detrended WASP-32 lightcurve from the SuperWASP data archive, observed in the date range interval 5048.57056713 − 5153.42813657 HJD and with planetary transits removed. The dashed line indicates the FAP of 0.1% and indicates the level where a period detection is defined. The peak period corresponds to $P_{\rm rot} = 11.6 \pm 1.0$ days and is at the 0.1% FAP power level. The peak at 5.8 days is a harmonic of the peak detected period.

4 CONCLUSIONS

The spectrosopic transits of WASP-13b and WASP-32b were observed with the SOPHIE spectrograph and the projected spin-orbit alignment was determined for both systems where $\lambda = 8^{\circ+13}_{-12}$ and $-2^{\circ+17}_{-19}$, respectively. WASP-13 and WASP-32 are consistent with alignment within 1σ. This suggests WASP-13 and WASP-32 had a gentle migration history and remained unperturbed from the original obliquity of the protoplanetary disk. An alternative scenario is the gradual loss of orbital energy by the planet through tidal dissipation, acting to realign the stellar spin and planetary orbital axes over a long enough timescale (Winn et al. 2010). The misalignment angle measured for WASP-32 in this work is consistent with the value of $\lambda = 10.5^{\circ+6.4}_{-6.5}$ measured by Brown et al. (2012). Our measured 3D alignment angle of $\psi = 11° \pm 14$ provides further evidence that the system is well-aligned. It is important to note that ψ has not been measured for many systems (see Table 2) and WASP-32 adds to the number of systems with a measured 3D alignment angle. Further, Table 2 shows that some systems are unambiguously aligned. Attempts have been made to derive the original obliquity distribution (Triaud et al., 2010; Li 2013) assuming a $\cos i_\star$ probability distribution in the stellar inclination, however this deprojection technique means that cases where $i_\star = 90°$ are unaccounted for. All current measurements of ψ in Table 2 show that there is a bimodal distribution in ψ: a planetary population that is aligned and one that is near isotropic. Thus, any attempt to deproject the population of spin-orbit angles is destined to fail if current trends in $i_\star$ are not recognised.

Winn et al. (2010) proposed one mechanism that could explain the observed distribution of alignment angles via tidal dissipation with the host star. In this scheme aligned planets are

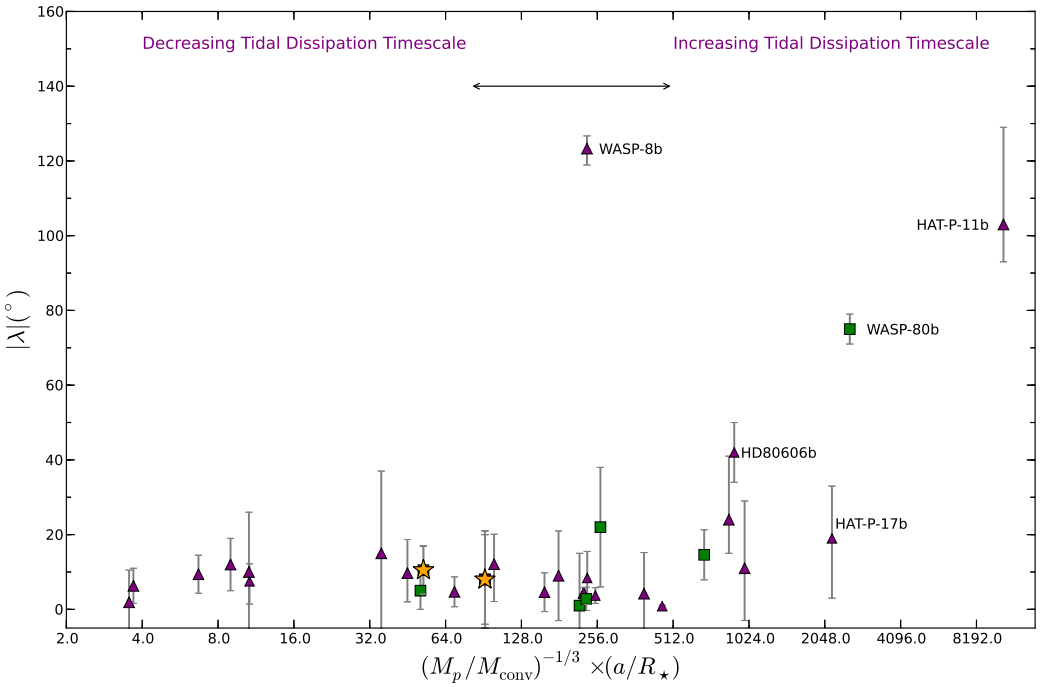

Figure 4. Plot of $|\lambda|$ against $(M_p/M_{\rm conv})^{-1/3} \times (a/R_\star)$ for all systems with $T_{\rm eff} < 6150$K. $a/R_\star$ is obtained directly from the planetary transit. The convective mass, $M_{\rm conv}$, was derived from the EZ-Web stellar evolution code.Systems with age determinations are shown as triangle symbols and those with an assumed age of 4 Gyrs are shown as square symbols. WASP-13b and WASP-32b are shown as starred symbols on the plot.

expected around cool stars ($T_{\rm eff} < 6250$K) and misaligned planets are expected orbiting hot host stars ($T_{\rm eff} > 6250$K). WASP-13 and WASP-32 have $T_{\rm eff} = 5989 \pm 48$K and $T_{\rm eff} = 6100 \pm 100$K, respectively, and therefore both lie in the cool regime. Thus both WASP-13 and WASP-32 add further evidence to alignment arising from tidal interactions. Also it must be noted that WASP-32 has a $T_{\rm eff}$ close to 6250K, perhaps indicating that it is possible for massive planets (in this case with a mass $> 3 M_{\rm J}$) to tidally realign around relatively hot host stars.

Alignment is expected to be determined by planet-star tidal interactions. The tidal interaction timescale due to tidal dissipation in the convective envelope is related to q, the planet to star mass ratio, and the scaled semi-major axis, $a/R_\star$ (see equation 2 of Albrecht et al. 2013):

$$\frac{1}{\tau_{\rm CE}} = \frac{1}{10 \times 10^9 {\rm yr}} q^2 \left(\frac{a/R_\star}{40}\right)^{-6} \quad (4)$$

Thus, the above equation shows that $\tau_{\rm CE} \propto q^{-2} \times (a/R_\star)^6$. As planet-star tidal interactions with the convective envelope are thought to be responsible for aligning hot-Jupiters via tidal dampening, we modified Equation 4 to include the convective mass of the planet host, $M_{\rm conv}$. Thus in Figure 4 an ensemble of systems with RM measurements are plotted against $(M_p/M_{\rm conv})^{-1/3} \times (a/R_\star)$, a quantity proportional to the tidal dissipation timescale. The convective envelope mass, $M_{\rm conv}$, was derived using the EZ-Web stellar evolution code [2]. To run the stellar models, the age of the system is required. For systems lacking derived ages, we have assumed an age of 4 Gyrs, but note the results are largely insensitive to age. Note the x-axis scale was chosen such that $\tau_{\rm CE}^{1/6} \propto (M_p/M_{\rm conv})^{-1/3} \times (a/R_\star)$ for plotting convenience. As suggested by Zahn (1977) tides are dissipated more effectively when the planet orbits a star with a convective envelope. Winn et al. (2010) have postulated that tides have changed the distribution of spin-orbit angles with $T_{\rm eff} < 6150$K but left the distribution unaltered with $T_{\rm eff} > 6350$K. Thus, only 'cool' systems with $T_{\rm eff} < 6150$K are plotted in Figure 4. It can be observed that as the tides become weaker (when the tidal dissipation timescale increases) there is some evidence that misaligned orbits are more likely. WASP-13 and WASP-32 are plotted in Figure 4 and are consistent with alignment. A recent addition to the ensemble of RM measurements is WASP-80b (Triaud et al. 2013), a K7-M0 star and the coolest host star in the sample with $T_{\rm eff} = 4145 \pm 100$K. Even as the coolest system, the planet is on an inclined circular orbit with $|\lambda| = 75^\circ$ similar to the spin-orbit angle measured around hotter mid-F stars. This suggests that hot-Jupiters may have been more frequently misaligned in the past. However, other mechanisms could act to misalign a system such as the presence of another peturbing body or if the host star is not old enough to develop a convective envelope. WASP-80b is considered a rare example of a misaligned system around a cool host star (Triaud et al. 2013). However, Figure 4 suggests that WASP-80b is yet to realign because of its long tidal dissipation timescale.

Even though the above analysis is simplified, Figure 4 suggests that planet-star tidal interactions likely play a role in damping the obliquities of hot-Jupiters around cool host stars.

[2] EZ-Web Stellar Evolution Code:
http://www.astro.wisc.edu/∼townsend/static.php?ref=ez-web

Table 2. Table of all cases where the 3D alignment angle, ψ, has been reported in the literature. The measured ψ and reference is indicated in the table. Multiple references indicate where ψ has been measured in seperate studies. Cases where multiple ψ measurements are listed with a single reference stems from orbital geometry degeneracies. Our result for WASP-32 adds to the number of systems with a complete 3D alignment angle determination.

Object	ψ (°)	Reference
CoRoT-18b	20 ± 20	[1]
HAT-P-7	> 86.1	[2]
HAT-P-11	$106^{+15}_{-11},\ 97^{+8}_{-4}$	[3]
Kepler-16(AB)b	< 18.3	[4]
Kepler-17b	0 ± 15	[5]
Kepler-63b	104^{+9}_{-14}	[6]
Kepler-13.01	$54 \pm 4,\ 56 \pm 4,\ 124 \pm 4,\ 126 \pm 4$	[7]
KOI-368.01	69^{+9}_{-10}	[8]
PTFO 8-86956b	73.1 ± 0.5	[9]
WASP-15b	> 90.3	[10]
WASP-17b	$> 91.7,\ > 92.6$	[10], [11]
WASP-19b	$< 19,\ < 20$	[10], [12]
WASP-32b	$\mathbf{11 \pm 14}$	**This Work**

[1] Hébrard et al. (2011b) **[2]** Winn et al. (2009) **[3]** Sanchis-Ojeda & Winn (2011) **[4]** Winn et al. (2011) **[5]** Désert et al. (2011) **[6]** Sanchis-Ojeda et al. (2013) **[7]** Barnes, Linscott & Shporer (2011) **[8]** Zhou & Huang (2013) **[9]** Barnes et al. (2013) **[10]** Triaud et al. (2010) **[11]** Bayliss et al. (2010) **[12]** Hellier et al. (2011)

Systems with short tidal dissipation timescales are preferentially aligned, however those with longer timescales show an apparent random distribution in λ. This may suggest that hot-Jupiters once had a broader range of obliquities in the past and, that they have been realigned over time via tidal interactions (Albrecht et al. 2013). In Figure 4, WASP-8b is the most obvious outlier in the distribution, however WASP-8 is a dynamically complex system with suggestions the Kozai mechanism or violent dynamical interations may explain the misaligned orbit (Queloz et al. 2010).

It is known that stars with $\mathrm{M} > 1.2\mathrm{M}_{\odot}$ cool as they evolve along the main sequence. As the star cools an outer convective envelope develops, increasing the strength of the tidal interactions. Thus the distribution of spin-orbit angles is expected to change with time where a planet originally on a misaligned orbit will realign as the convective envelope of the host star develops. Triaud 2011 plotted $|\lambda|$ against age for all systems with $\mathrm{M} > 1.2\mathrm{M}_{\odot}$. The plot provides weak evidence that the spin-orbit alignment distribution changes with time and is another manifestation of the influence of tidal interactions. Objects with ages 2.5-3 Gyrs appear aligned, whereas more misaligned systems are observed around stars with younger ages. Even though the plots of $|\lambda|$ against $a/R_{\star}$ and age show evidence for evolution due to tides, it is still unclear if an original misaligned hot-Jupiter population would survive realignment around 'cool' host stars or tidally infall into the star, leaving the aligned population observed today.

We have presented RM measurements for WASP-13 and WASP-32. Analysing out-of-transit survey photometry for WASP-32 revealed the rotation period of the host star, and thus the 3D alignment angle $\psi = 11^{\circ} \pm 14$ of the planetary system. WASP-32 adds to the number of systems with a full 3D alignment angle determination. It is clear that it is becoming increasingly important to investigate the full star-planet-disk (e.g., Watson et al. 2011; Kennedy et al. 2013) alignment in order to fully assess the migration history of exoplanets. Only with an alignment determination of the whole system can we begin to fully evaluate the migration scenarios of hot-Jupiters.

ACKNOWLEDGMENTS

We thank J. Southworth for making his JKTLD code available for calculating limb darkening coefficients. This research has made use of the Astrophysics Data System (ADS), the Extrasolar Planets Encyclopaedia, R. Heller's Holt Rossiter-McLaughlin Encyclopaedia and R. Townsend's EZ-Web stellar evolution code. R. D. B. acknowledges support from the Queen's University Belfast Department for Education and Learning (DEL) university scholarship. C.A.W. acknowledges support by STFC grant ST/I001123/1. All RM observations were taken with the SOPHIE spectrograph on the 1.93 m telescope at Observatoire de Haute-Provence (CNRS), France. WASP-13 was observed as part of directors discretionary time and WASP-32 as part of OPTICON time. R. D. B. acknowledges the complementary analysis of WASP-13 and WASP-32 RM observations by Élodie Hébrard using an RML fitting routine. This provided a consistency check of our determined obliquities. Also R. D. B. would like to thank D. R. Anderson for simultaneously fitting the photometry and RVs for all our targets, providing a further consistency check. R. D. B. would like to thank Armaury Triaud for useful advice that greatly enhanced the discussion in this report. We would also like to thank the anonymous referee for their careful reading and detailed comments on the paper.

REFERENCES

Albrecht S. et al., 2012, ApJ, 757, 18
Albrecht S., Winn J. N., Marcy G. W., Howard A. W., Isaacson H., Johnson J. A., 2013, ApJ, 771, 11
Barnes J. W., Linscott E., Shporer A., 2011, ApJS, 197, 10
Barnes J. W., van Eyken J. C., Jackson B. K., Ciardi D. R., Fortney J. J., 2013, ApJ, 774, 53
Bate M. R., Lodato G., Pringle J. E., 2010, MNRAS, 401, 1505
Bayliss D. D. R., Winn J. N., Mardling R. A., Sackett P. D., 2010, ApJ, 722, L224
Brown D. J. A. et al., 2012, ApJ, 760, 139
Claret A., 2004, A&A, 428, 1001
Désert J.-M. et al., 2011, ApJS, 197, 14
Gaudi B. S., Winn J. N., 2007, ApJ, 655, 550
Goldreich P., Tremaine S., 1980, ApJ, 241, 425
Gómez Maqueo Chew Y. et al., 2013, ApJ, 768, 79
Greaves J. S. et al., 2014, MNRAS, 438, L31
Hébrard G. et al., 2011a, A&A, 527, L11
Hébrard G. et al., 2011b, A&A, 533, A130
Hellier C., Anderson D. R., Collier-Cameron A., Miller G. R. M., Queloz D., Smalley B., Southworth J., Triaud A. H. M. J., 2011, ApJ, 730, L31
Hirano T. et al., 2012, ApJ, 759, L36
Horne J. H., Baliunas S. L., 1986, ApJ, 302, 757
Huber D. et al., 2013, ArXiv e-prints
Kennedy G. M., Wyatt M. C., Bryden G., Wittenmyer R., Sibthorpe B., 2013, MNRAS, 436, 898

Kozai Y., 1962, ApJ, 67, 591
Lai D., Foucart F., Lin D. N. C., 2011, MNRAS, 412, 2790
Lidov M. L., 1962, Planet. Space Sci., 9, 719
Lin D. N. C., Bodenheimer P., Richardson D. C., 1996, Nat, 380, 606
Lomb N. R., 1976, Astrophys. Space. Sci., 39, 447
Maxted P. F. L. et al., 2010, PASP, 122, 1465
Moutou C. et al., 2011, A&A, 533, A113
Ohta Y., Taruya A., Suto Y., 2005, ApJ, 622, 1118
Queloz D. et al., 2010, A&A, 517, L1
Saar S. H., Donahue R. A., 1997, ApJ, 485, 319
Sanchis-Ojeda R., Winn J. N., 2011, ApJ, 743, 61
Sanchis-Ojeda R. et al., 2013, ApJ, 775, 54
Scargle J. D., 1982, ApJ, 263, 835
Simpson E. K., Baliunas S. L., Henry G. W., Watson C. A., 2010, MNRAS, 408, 1666
Simpson E. K. et al., 2011, MNRAS, 414, 3023
Skillen I. et al., 2009, A&A, 502, 391
Triaud A. H. M. J., 2011, A&A, 534, L6
Triaud A. H. M. J. et al., 2013, A&A, 551, A80
Triaud A. H. M. J. et al., 2010, A&A, 524, A25
Walkowicz L. M., Basri G. S., 2013, MNRAS
Watson C. A., Littlefair S. P., Collier Cameron A., Dhillon V. S., Simpson E. K., 2010, MNRAS, 408, 1606
Watson C. A., Littlefair S. P., Diamond C., Collier Cameron A., Fitzsimmons A., Simpson E., Moulds V., Pollacco D., 2011, MNRAS, 413, L71
Winn J. N. et al., 2011, ApJ, 741, L1
Winn J. N., Fabrycky D., Albrecht S., Johnson J. A., 2010, ApJ, 718, L145
Winn J. N., Johnson J. A., Albrecht S., Howard A. W., Marcy G. W., Crossfield I. J., Holman M. J., 2009, ApJ, 703, L99
Zahn J.-P., 1977, A&A, 57, 383
Zhou G., Huang C. X., 2013, ApJ, 776, L35

Table 3. Radial velocities and 1σ error bars of WASP-13 measured with *SOPHIE* during and outside transit.

BJD -2 400 000	RV (km s^{-1})	Error (km s^{-1})
5993.31409	9.7904	0.0145
5993.32150	9.8080	0.0146
5993.32902	9.8182	0.0155
5993.33602	9.8084	0.0141
5993.34263	9.8009	0.0140
5993.34859	9.8145	0.0137
5993.35443	9.8019	0.0140
5993.36088	9.8099	0.0139
5993.36932	9.7990	0.0143
5993.37564	9.7856	0.0134
5993.38098	9.7665	0.0135
5993.38634	9.7953	0.0134
5993.39186	9.8092	0.0135
5993.39793	9.7967	0.0135
5993.40506	9.7772	0.0137
5993.41112	9.7625	0.0137
5993.41708	9.7577	0.0135
5993.42317	9.7603	0.0136
5993.42985	9.7796	0.0140
5993.43624	9.7763	0.0137
5993.44225	9.7706	0.0137
5993.44745	9.7376	0.0136
5993.45216	9.7776	0.0133
5993.45649	9.7616	0.0132
5993.46069	9.7642	0.0131
5993.46483	9.7555	0.0130
5993.47332	9.7646	0.0128
5993.47773	9.7833	0.0128
5993.48256	9.7792	0.0132
5993.48852	9.7982	0.0139
5993.49531	9.7980	0.0141
5993.50170	9.7743	0.0136
5993.50820	9.7951	0.0136
5993.51431	9.7916	0.0135
5993.52041	9.7521	0.0134
5993.52615	9.7550	0.0133
5993.53177	9.7796	0.0133
5993.53739	9.7534	0.0132
5993.54392	9.7606	0.0134
5993.54966	9.7866	0.0137
5993.55566	9.7685	0.0136
5993.56168	9.7801	0.0134
5993.56763	9.7688	0.0137
5993.57412	9.7764	0.0140
5993.58127	9.7691	0.0137
5993.58813	9.7442	0.0139
5993.59483	9.7579	0.0137
5993.60164	9.7778	0.0143
5993.60865	9.7475	0.0140
5993.61494	9.7584	0.0137
5993.62145	9.7903	0.0142
5993.62827	9.7537	0.0153
5993.63558	9.7447	0.0148
5993.64269	9.7797	0.0145

Table 4. Radial velocities and 1σ error bars of WASP-32 measured with *SOPHIE* during and outside transit.

BJD -2 400 000	RV (km s^{-1})	Error (km s^{-1})
5803.44375	18.2586	0.0230
5803.45634	18.2510	0.0229
5803.46888	18.2249	0.0231
5803.47919	18.2285	0.0225
5803.48888	18.2439	0.0230
5803.49942	18.2344	0.0231
5803.50922	18.2643	0.0224
5803.51874	18.2419	0.0222
5803.52952	18.2165	0.0228
5803.54057	18.1203	0.0217
5803.55190	18.1145	0.0221
5803.56303	18.0880	0.0225
5803.57313	18.1301	0.0219
5803.58378	18.1474	0.0213
5803.59428	18.0968	0.0216
5803.60508	18.0819	0.0214
5803.61574	18.0997	0.0218
5803.62640	18.0852	0.0220
5803.63663	18.0709	0.0220
5803.64635	18.0726	0.0224
5803.65582	18.0417	0.0222
5803.66534	18.0676	0.0298

Table 5. Derived system parameters and uncertainties for WASP-13. The effective temperature is taken from Gómez Maqueo Chew et al. (2013). Fitted free parameters are listed with the corresponding errors followed by the parameters controlled by priors (listed in Equation 2).

Parameter (units)	Symbol	Value
Free parameters:		
Projected alignment angle ($^\circ$)	λ	8^{+13}_{-12}
Projected stellar rotation velocity (km s^{-1})	$v \sin i$	5.7±0.4
RV semi-amplitude (km s^{-1})	K	0.0564±0.0043
Systemic velocity of SOPHIE transit dataset (km s^{-1})	$\gamma_{\rm transit}$	9.7854±0.0037
Systemic velocity of SOPHIE orbital dataset (km s^{-1})	$\gamma_{\rm orbit}$	9.8345±0.0031
Parameters controlled by priors:		
Period (days)	P	4.3530135±0.000003
Transit epoch ($\rm BJD_{UTC}$ - 2 400 000)	T_0	5304.53998±0.00025
Planet/Star radius ratio	R_p/R_*	$0.0918^{+0.0127}_{-0.0126}$
Scaled semi-major axis	a/R_*	7.54±0.27
Orbital inclination ($^\circ$)	i	85.43±0.29
Fixed parameters:		
Eccentricity	e	0
Limb darkening	u	0.75
Effective temperature (K)	$T_{\rm eff}$	5989 ±48

Table 6. Derived system parameters and uncertainties for WASP-32. The effective temperature is taken from Maxted et al. (2010)

Parameter (units)	Symbol	Value
Free parameters:		
Projected alignment angle (°)	λ	-2^{+17}_{-19}
RV semi-amplitude (km s^{-1})	K	$0.4789^{+0.0079}_{-0.0078}$
Systemic velocity of SOPHIE transit dataset (km s^{-1})	$\gamma_{\rm transit}$	18.1698±0.0095
Systemic velocity of SOPHIE orbital dataset (km s^{-1})	$\gamma_{\rm orbit}$	$18.2796^{+0.0061}_{-0.0062}$
Parameters controlled by priors:		
Projected stellar rotation velocity (km s^{-1})	$v \sin i$	3.9 ±0.5
Period (days)	P	2.7186590±0.000008
Transit epoch (HJD - 2 400 000)	T_0	5150.39051±0.00050
Planet/Star radius ratio	R_p/R_*	0.1091±0.0010
Scaled semi-major axis	a/R_*	7.63±0.35
Orbital inclination (°)	i	85.30±0.50
Fixed parameters:		
Eccentricity	e	0.018 ±0.0065
Limb darkening	u	0.71
Effective temperature (K)	$T_{\rm eff}$	6100 ± 100